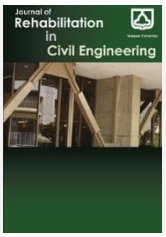

Journal of Rehabilitation in Civil Engineering

Journal homepage: https://civiljournal.semnan.ac.ir/

Evaluation of Human Interventions on Longshore Sediment Transport in Damietta Port Area

Ahmed S.A. Ibrahim [1,*]; Anas M. El-Molla [1]; Hany G.I. Ahmed [1]

1. Department of Civil Engineering, Faculty of Engineering, Al-Azhar University, Cairo, Egypt
* Corresponding author: *ahmedsayed.90@azhar.edu.eg*

ARTICLE INFO

Article history:
Received:
Revised:
Accepted:

Keywords:
Coastal hazard;
Wave climate;
Long-term trend;
Sediment transport;
MIKE21SM.

ABSTRACT

Coastal regions are increasingly vulnerable to climate change-induced hazards such as erosion, with the combination of environmental threats and human activities exacerbating the vulnerability of these ecosystems. The study, spanning eight decades (i.e. 1940-2020), utilizes ECMWF-ERA5 data and a high-resolution model (MIKE21 SM) to simulate Longshore Sediment Transport (LST) in response to human interventions. Model accuracy is validated against observed data from the Damietta buoy and 2011 bathymetry data. Additionally, comparisons with the estimated LST from previous regional studies confirm the model's reliability. The investigation focuses on identifying trends in LST before and after human interventions, including the construction of Damietta Port (DP) and subsequent coastal protection structures. Two different trend analysis methods, linear regression and Theil-Sen, are used to capture temporal variations in LST. According to Theil-Sen, trend values increased as a result of the port construction, with Gross LST (GLST) and Net LST (NLST) increasing by 100-160%, respectively. However, both GLST and NLST experienced significant decreases following coastal protection (i.e. 27-24%, respectively). Moreover, the correlation analysis of wave parameters and LST revealed a variety of relationships over periods, illustrating the complicated relationship between sediment transport processes and human activities. Notably, prior to the construction of DP, there were strong correlations between NLST, wave height, and peak wave period (i.e. R=0.81-0.79, respectively), but these decreased significantly after construction (i.e. R=0.59-0.60). Following coastal protection, correlations with sediment transport increased (i.e. R=0.79-0.77).

E-ISSN: 2345-4423

How to cite this article:
Ibrahim, A., El Molla, A., & Ahmed, H. (2024). Evaluation of Human Interventions on Longshore Sediment Transport in Damietta Port Area. Journal of Rehabilitation in Civil Engineering, 12(3), 85-96. https://doi.org/10.22075/jrce.2024.32512.1948

1. Introduction

Sustainable coastal management is gaining global significance in areas that cover three-quarters of the earth's surface, where burgeoning populations and activities of people have tended to put pressure on this region [1]. The dynamics of coastal regions have changed over extended historical epochs to the present day due to human activity and climate change. Furthermore, threats associated with climate change, such as increased wave activity, erosion, and flooding, are exacerbated by human activity [2–4]. Erosion is one of the issues, which is exacerbated by these areas' dense populations [5]. LST is mainly driven by wave-induced mechanisms that shape the coastline [6,7].

Researchers studied the LST mechanism's effects and significance on changes in coastal morphology, concurrently investigating methodologies and calculation procedures for monitoring these shifts [8–10]. For efficient coastal management, planning, and maintenance, numerical simulations of hydrodynamics, LST and morphological transformations are crucial [11]. Numerical models are essential for predicting wave events, designing structures and assessing coastal hazards [12,13]. It enables researchers and engineers to simulate and evaluate complicated oceanic and coastal phenomena. However, these models need refinement and verification to improve their accuracy and reliability. This is because waves, ocean currents and atmospheric conditions all interact in ways.

The Mediterranean area is experiencing accelerated temperature rises that further increase erosion risk due to intense waves [14]. The Mediterranean Sea, a closed basin [15], has been widely exploited by humans, further exacerbating its vulnerability to natural hazards [16]. The potential hazards caused by climate change to ports, which are critical elements of global trade, have received insufficient attention, particularly in Egypt [17]. Coastal engineers presently grapple with the challenge of accurately estimating and predicting critical factors, including nearshore waves and LST [18]. Examining the previously neglected Egyptian coast can help coastal engineers expand their knowledge base, particularly when it comes to critical factors like nearshore waves and LST [19]. This research gap highlights the importance of studying and understanding the specific challenges and vulnerabilities that Egyptian ports may face as a result of human interventions and climate change.

In this study, the ECMWF-ERA5 dataset, spanning eighty-one years from 1940 to 2020, is employed to explore long-term trends and patterns in the climate. It is broken down into three stages, each of which concentrates on a distinct era linked to the development of DP and coastal structures. The study objective is to assess the impact of human interventions on LST through a multifaceted approach that includes numerical modelling, long-term trend analysis, and wave-LST correlation analysis.

2. Materials and methods

2.1. Study area

The study focuses on DP, an important maritime project in the Mediterranean Sea [20]. Its location was chosen because of its history of shoreline accretion [21,22]. DP is situated in the Nile Delta and was established in 1982. It consists of two jetties and is approximately 9.7 km west of the Damietta Nile branch. [23]. In response to coastal erosion, authorities installed eight detached breakwaters along the Ras El-Bar coast between 2003 and 2004 [24]. Additionally, from 2016 to 2019, extensive coastal protection efforts were carried out with the construction of T-detached breakwaters. Since 2021, continuous development activities have been underway at DP. A new jetty,

approximately 3.0 km long, has been constructed west of the port. An extension to the eastern jetty, measuring approximately 1.4 km, has also been implemented.

2.2. Data collection

The study scope encompasses the coastal area surrounding DP, spanning a length of 10 km. The initial bathymetric data for this region was derived from profiles collected in 2010. For calibration and verification of our model, wave data were collected from a buoy situated at 31°51'N, 31°76'E off the DP coast, positioned 12 m deep (Figure 1). This dataset spans two years, covering wave measurements from 2003 to 2004, with readings taken at four-hour intervals. To enhance the precision and reliability of our model, an additional set of four bathymetric profiles was gathered from the field in 2011. These profiles were critical in calibrating and verifying the model, resulting in an accurate simulation of depths. Notably, at the Nile Delta, the tidal range is consistently low, averaging only 0.14 m over the past two decades, with a daily fluctuation of 0.60 m [25]. Moreover, grain size measurements reveal a decrease in D50 values from the beach towards the open sea, with beach values averaging about 0.25 mm. Sediments on the seabed up to a depth of six m exhibit approximately 0.11 mm [26].

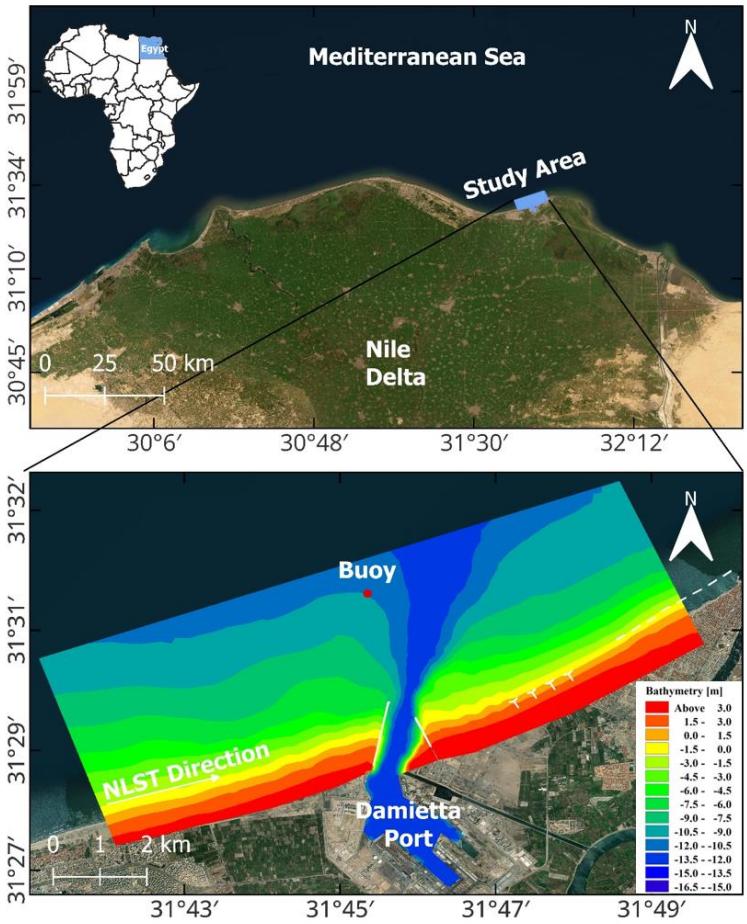

Fig. 1. Study area map shows the location, bathymetry, wave buoy, and coastal structures.

2.3. Numerical Model

The Danish Hydraulic Institute (DHI) developed the MIKE21 Shoreline Morphology model, which was used as the primary tool in this study. The primary objective was to create a hybrid model integrating hydrodynamic and sediment transport components within the MIKE21 program framework. The software

consists of four main modules: Spectral Wave (MIKE21 SW), Hydrodynamic (MIKE21 HD), and Shoreline Morphology (MIKE21 SM) [27].

MIKE21 HD module solves equations related to mass momentum salinity and temperature [28]. MIKE21 SW is a model specifically developed for simulating two-dimensional 2D waves in coastal and offshore settings [29]. It utilizes a computational mesh that uses a finite volume technique grounded in the differential equations governing ocean wave dynamics [30,31]. The equations are stated as follows:

$$\frac{S}{\sigma} = \frac{\partial N}{\partial t} + \nabla(\vec{v}N) \quad (1)$$

where: t: time, $v = (c_\sigma, c_\theta, c_x, c_y)$: propagation velocity in *4-D*, $N(\sigma, \theta, x, t)$: Represents the action-density, x and y: is the Cartesian-coordinates, and ∇: 4-D spatial differential operator (i.e. v, σ, and θ).

MIKE21 ST is responsible for simulating sediment transport and takes into consideration currents interactions as well as turbulence, sediment concentration, and flow velocity. It computes bed load and suspended load transport, utilizing the Shields parameter and flow velocities. Vertical fluctuations in sediment concentration are determined using a diffusion equation. The MIKE21 SM shoreline continuity equation considers the effects of the results, particularly littoral drift gradients, on shoreline morphology. The one line theory, which separates the shoreface into perpendicular strips and determines shoreline position by integrating changes in sediment amount within each strip, is used in this equation. [32].

$$\frac{\Delta N}{\Delta t} = \frac{vol}{dA_z} \quad (2)$$

where: ΔN is used to signify the horizontal distance by shoreline moves in a direction perpendicular to the shore. *dAz* is the vertical area of the active profile within each shore face strip, and it is the area over which sediment (*vol*) is evenly distributed. Δt is the time step.

2.4. Model calibration and verification

Model calibration and verification procedures were carried out to assess the model's accuracy with important parameters within the study region. Three parameters are under investigation: wave height (H_s), wave period (T_p), and bed level. While data from the Damietta buoy in 2003 was used for model calibration, observed results from the same buoy in 2004 were examined for model verification. Depth data collected in 2011 was used for both calibration and verification purposes.

Figure 2 depicts the procedures used to calibrate and verify the MIKE21 model. To evaluate the model's performance, we used statistical metrics such as correlation coefficient (CC), root mean square error (RMSE), bias, and scatter index (SI). Bias quantifies the difference between the model's predicted average values and the values observed on-site. The following equations apply to the parameters:

$$\bar{x} = \frac{1}{n}\sum_{i=1}^{n} x \quad (3)$$

$$\bar{y} = \frac{1}{n}\sum_{i=1}^{n} y \quad (4)$$

$$CC = \frac{\sum_{i=1}^{n}(x_i-\bar{x})(y_i-\bar{y})}{\sqrt{\sum_{i=1}^{n}(x_i-\bar{x})^2 \sum_{i=1}^{n}(y_i-\bar{y})^2}} \quad (5)$$

$$RMSE = \sqrt{\frac{1}{n}\sum_{i=1}^{n}(y-x)^2} \quad (6)$$

$$BIAS = \frac{1}{n}\sum_{i=1}^{n}(y-\bar{x}) \quad (7)$$

$$SI = \frac{\sqrt{\frac{1}{n}\sum_{i=1}^{n}(y-x-BIAS)^2}}{\frac{1}{n}\sum_{i=1}^{n}|x_i|} \quad (8)$$

Where: n represents the number of data, x is the measured value, y is the simulated value, and x and y represent the average values.

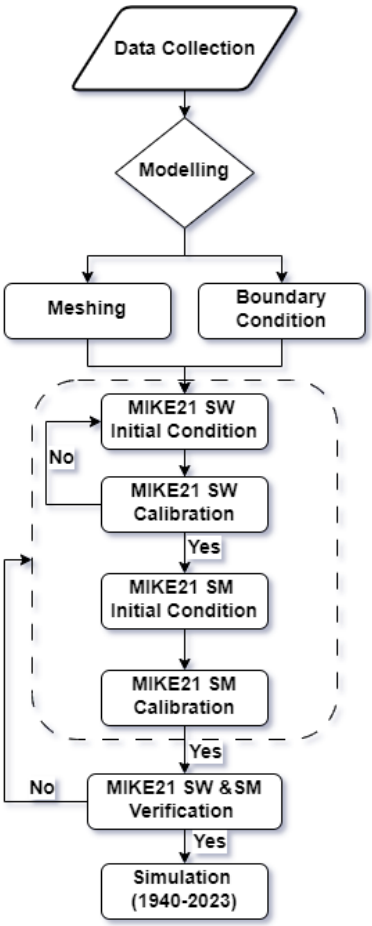

Fig. 2. Flowchart for the model calibration and verification process.

2.5. Long-term trend in LST

Assessing long-term trends in sea state is an evolving area of research. Through our analysis, we have identified yearly trends in LST. This study uses two distinct methodologies for time series analysis to detect trend patterns within the LST dataset. These methodologies include the use of linear regression and Theil-Sen estimation. Following that, a detailed description of the methods used, as well as the results obtained from each approach, will be provided.

2.5.1. Linear regression

Linear regression is a statistical method for modelling the relationship between variables by fitting a linear equation to the data. It seeks to identify the best-fitting straight line that describes the linear relationship between variables. The line equation is represented as follows:

$$y = a + b * t \tag{9}$$

where y represents the LST, t denotes time, and a and b are the regression coefficients.

2.5.2. Theil-Sen estimator

Theil-Sen estimator is a nonparametric technique for calculating the slope of a linear relationship between two variables. It computes the median of the slopes of all possible pairs of points in the dataset, resulting in a stronger estimate of the slope that is less affected by outliers than traditional linear regression methods [33,34]. Theil-Sen is more reliable because it is less sensitive to extreme values [35]. The Theil-Sen method's slope estimation formula is as follows:

$$Slop = \text{Median}\left(\frac{y_i - y_j}{t_i - t_j}\right) \tag{10}$$

where y represents the LST at time t_i *and* t_j ($t_i > t_j$).

3. Results and discussion

3.1. Model calibration and verification

Throughout the calibration phase, it became apparent that the model consistently achieved robust correlation values when compared to the observed values for all parameters. Specifically, the CC stood at 0.93, while for bed levels, the CC reached 0.99. Furthermore, the RMSE values consistently remained low, signifying a strong agreement between measured and simulated parameters. Nevertheless, certain instances did reveal a minor bias, particularly in Hs, where a negative bias of -0.03 was observed. During verification, the model maintained a high correlation with observed data, though some parameters exhibited slightly higher RMSE values (table 1). It's important to note that some parameters exhibited slightly higher RMSE values. Overall, the model accurately predicts critical parameters in the study area, with a strong agreement between modelled and observed parameters.

Table 1. Statistical metrics between simulated and observed parameters in the study area.

Parameters	Calibration				Verification			
	CC	Bias	RMSE	SI (%)	CC	Bias	RMSE	SI (%)
Wave height (m)	0.93	0.03	0.18	0.29	0.9	-0.03	0.23	0.31
Wave period (s)	0.78	-0.29	1.04	0.15	0.72	-0.19	1.26	0.19
Bed level (m)	0.99	0.05	0.21	0.04	0.99	0.09	0.21	0.04

3.2. Wave climate

Analysis of simulated wave data from 1940 to 2020 revealed that waves primarily originate in the N-NW sector, accounting for 86% of all observed wave directions. Previous researchers have reported similar findings [36,37]. Figure 3 shows the monthly wave rose, simulated using MIKE 21 and spans 81 years. H_s data extracted from the MIKE21 SW model at a depth of 12 m from the DP coastline reveal H_s variability ranging from 0.01-4.94 m. The T_p ranged from 2.00 to 14.30 seconds, with a predominant direction of 326°. The 81-year monthly averages of wave parameters show that during the winter season, Hs ranges from 0.55 to 1.55 m, with an average of 1.03 m, and T_p ranges from 5.40 to 8.10 seconds. In contrast, during the summer, H_s ranges from 0.61 to 1.28 m and T_p from 4.90 to 7.00 seconds. The average H_s along the study area's coast in spring and autumn is 0.85 m. Monthly variations in H_s show that the highest maximums occur between November and March. H_s less than 1.00 m occur more than 68% of the year. H_s between 1.00 and 2.00 m account for roughly 28% of all times, while H_s greater than 2.00 m account for about 0.04% of the time.

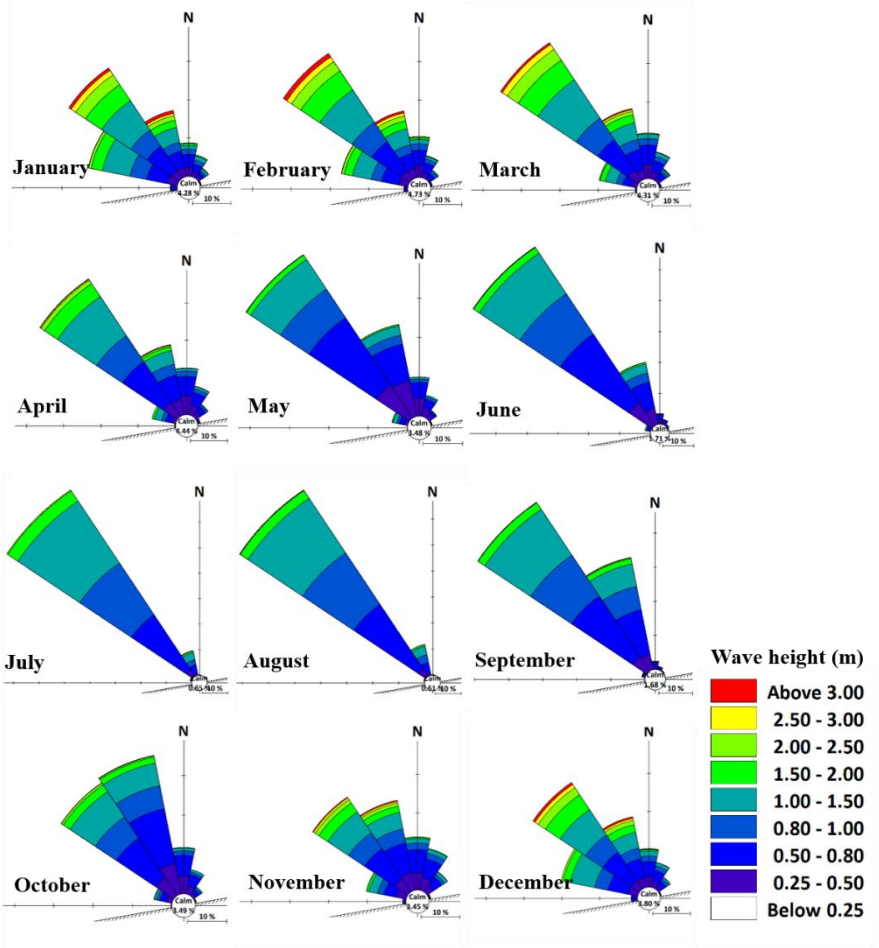

Fig. 3. Monthly wave rose over 81 years (1940–2020).

3.3. Longshore sediment transport

Transport rates vary temporally and spatially, depending on the orientation of the Hs and the seasonal variations in the local wave climate. Consequently, an extensive analysis spanning 81 years was carried out to evaluate LST variability. As a result, recent human activity in the region has seriously disrupted the natural equilibrium of the available sediment budget, leading to notable changes in LST (Figure 4).

Notably, from 1940 to 1981, humans did not affect nearshore LST patterns, allowing sediments to move naturally. During this period, annual GLST fluctuated between 0.87 and 1.5 million m³, with an average of 1.1 million m³, while NLST varied between 0.49 and 1.04 million m³, with an average of 0.73 million m³. These estimates agree with previous findings in the study area. For instance, before the DP's construction, sediment transport was estimated at around 0.66 million m³/yr to the east and 0.26 million m³/yr to the west, resulting in an NLST of 0.4 million m³/yr to the east [22]. Other estimates for NLST included 0.8 million m³/yr [38] and a range of 0.6 to 1.8 million m³/yr [39].

However, because the DP jetties blocked sediment flow, LST values downstream of DP saw a sharp decline after DP construction. The maximum annual GLST was 1.07 million m³, while the lowest was 0.75 million m³. However, NLST varied from a low of 0.25 million m³ in 1982 to a peak of 0.65 million m³. In contrast, the NLST averaged 0.42 million m³/yr, while the GLST was approximately 0.9 million m³/yr. Furthermore, these results agree with the Frihy et al. study conducted after DP construction. According to this study, NLST is approximately 0.49 million m³/yr along the coastline, compared to GLST of approximately 0.85 million m³/yr [37].

After the construction of protective structures in the eastern part, there were notable annual fluctuations in LST. The maximum GLST was 1.07 million m³, the minimum was 0.75 million m³, and the average was around 0.9 million m³. Furthermore, the maximum NLST is 0.65 million m³. In contrast, the initial year of construction had the lowest observed NLST value of 0.25 million m³. The average annual NLST for this period was around 0.42 million m³/yr.

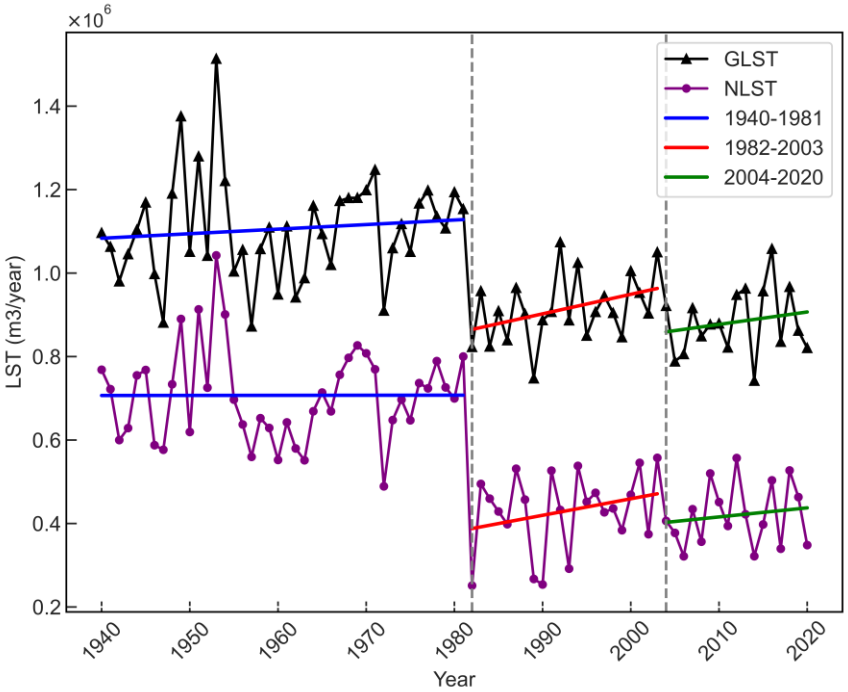

Fig. 4. Annual variation in LST over 81 years (1940–2020).

3.4. Analysis of long-term trends in LST

This section presents the LST trend analysis results for the DP coast, which were conducted using linear regression and Theil-Sen. Although both methods show consistent trends in LST prior to and following human interventions, this suggests that they are effective at capturing temporal variations. In contrast, both methods produce positive trends over the study periods, even though the magnitudes vary. The first step is to apply linear regression to investigate LST trends prior to and following the DP construction and subsequent coastal protection. Table 2 shows the linear regression results for LST trends throughout the study periods.

The results indicated that before the port's construction (1940–1981), GLST and NLST showed very slight trends, with 1140 m³/yr and 244 m³/yr, respectively. However, significant increases in both GLST and NLST trends were observed after DP (1982–2003), with GLST rising to 4680 m³/yr and NLST reaching 3962 m³/yr. However, there was a noticeable drop in both GLST and NLST trends after the installation of coastal protection structures (2004-2020). Likewise, GLST decreased to 2978 m³/yr and NLST to 2176 m³/yr, respectively.

Table 2. Linear regression slopes for annual LST data.

Period	Trend	Slop (m³/yr)	
		GLST	NLST
1940-1981	+ve	1140	244
1982-2003	+ve	4680	3962
2004-2020	+ve	2978	2176

Following that, LST data from all study periods were used to estimate long-term trends using the Theil-Sen method. In Table 3, the estimated trends based on yearly LST values are illustrated. As shown in Table 3, the analysis revealed significant changes in LST trends.

Prior to the DP construction, GLST and NLST had positive trends of 2190 and 990 m³/yr, respectively. However, GLST and NLST trends increased significantly during the DP's construction, reaching 4400 and 2560 m³/yr, respectively. However, both GLST and NLST trends have decreased substantially due to the construction of coastal protection structures. Likewise, GLST decreased to 3210 m³/year and NLST to 1940 m³/year.

Notable is the apparent increase in GLST trends, which increased by nearly 100% following the implementation of DP. Following the installation of protective structures, GLST trends were declined by 27%. In terms of NLST, there was a significant increase of 160% following the DP construction, followed by a 24% decrease after the beginning of coastal protection.

Table 3. Theil-Sen slopes for annual LST data.

Period	Trend	Slop (m³/yr)	
		GLST	NLST
1940-1981	+ve	2190	990
1982-2003	+ve	4400	2560
2004-2020	+ve	3210	1940

Based on previous results of linear regression and Theil-Sen for trend analysis of LST data, both methods show changes in LST values over time. Both approaches show a significant increase in both GLST and NLST trends following the construction of DP, indicating a significant disruption in LST. In contrast, after the construction of coastal protection structures, both methods show a decline in GLST and NLST trends, indicating that these structures helped to stabilise sediment dynamics and mitigate the effects of human activities.

Both linear regression and the Theil-Sen provide valuable information on LST data

trends and how they respond to human interventions. For example, before the construction of DP, linear regression shows a GLST trend of 1140 m³/yr, while the Theil-Sen method shows a significantly higher value of 2190 m³/yr. Similarly, for NLST during the same period, linear regression reports a slope of 244 m³/yr, while the Theil-Sen method shows a higher value of 990 m³/yr. These differences emphasise the estimation method's sensitivity to dataset characteristics, particularly outliers and data distribution. However, Theil-Sen provides more accurate estimates of trends, being less influenced by outliers in the data, which is evident in the smaller differences between trend values compared to linear regression.

3.5. LST and wave climate analysis

Furthermore, the study investigated the relationships between GLST, NLST, and wave climate. This analysis is used in the study to evaluate how human activities affect coastal dynamics and sediment transport processes. The correlation values (R) in Table 4 demonstrate interesting patterns in the association between wave parameters and LST over the study period. For example, during the pre-port building phase, H_s and T_p had good correlations with GLST at 0.92 and 0.84, respectively, and NLST at 0.81 and 0.79. After DP construction, there was a noticeable shift in correlation values, particularly for NLST. Notably, the correlation between NLST and Hs declined to 0.59, whereas NLST and T_p declined to 0.60.

In contrast, H_s and T_p showed positive correlations with GLST (0.96 and 0.85, respectively) and NLST (0.79 and 0.77, respectively) during the post-coastal protection structures phase. This demonstrates the effectiveness of these structures in restoring some aspects of the natural balance of LST.

These correlation values demonstrate the complicated relations between wave characteristics and sediment transport patterns along the coast, emphasizing how varied human interventions affect these correlations. Understanding these relationships is essential for understanding coastal dynamics and LST processes, which significantly affect coastal management and sustainable development.

Table 4. Wave parameter correlation coefficient (R) with LST throughout the study periods.

Wave parameter	1940-1981		1982-2003		2004-2020	
	GLST	NLST	GLST	NLST	GLST	NLST
H_s	0.92	0.81	0.94	0.59	0.96	0.79
T_p	0.84	0.79	0.82	0.60	0.85	0.77

4. Conclusion

The study highlights that human coastal interventions have significant effects on LST patterns. Using an extensive 81-year wave dataset, the study provides unique insights into the area's coastal dynamics. The construction of DP has disrupted the natural equilibrium of sediment transport, resulting in erosion and deposition changes along the coastline. However, coastal protection structures have been crucial in mitigating these effects and contributing to a more balanced shoreline, particularly on the eastern side of the port.

The study used two independent methods, linear regression and Theil-Sen, to identify trends in LST. Consistently positive trends were revealed both before and after human interventions in the trend analysis carried out using Theil-Sen and linear regression. However, Theil-Sen provides more accurate estimates of trends, being less influenced by

outliers in the data. The Theil-Sen results highlighted that trend values increased due to the construction of the port, with GLST rising from 2190 m^3/yr to 4400 m^3/yr and NLST rising from 990 m^3/yr to 2560 m^3/yr. However, both GLST and NLST experienced significant decreases following coastal protection (3210-1940 m^3/yr, respectively).

Additionally, correlation analysis revealed dynamic relationships between wave parameters and sediment transport patterns, underscoring the importance of understanding these interactions for coastal management. The correlations between wave parameters and LST demonstrate the intricate relationships influenced by human interventions. Understanding the implications of these development projects is crucial for coastal management and sustainable development efforts. The study highlights the importance of a comprehensive approach that considers both the short-term effects of construction and the long-term consequences for coastal morphology. The planning and implementation of new infrastructure projects are expected to change the morphology of the coast and sediment transport patterns, potentially increasing susceptibility to coastal hazards. Without proactive measures in place to manage sediment effectively, these developments may further exacerbate the degradation of coastal environments and compromise the resilience of coastal areas.

Based on this study, the following is recommended for future study:

More research is needed to develop a comprehensive strategy that considers the short- and long-term impacts of construction on coastal morphology. Additionally, identifying other factors that influence coastal dynamics is critical. For example, investigate the effects of rising sea levels, changing wave climates, and extreme events on coastal morphology and sediment transport patterns. By continuing to investigate these factors, we will gain a better understanding of how to address the challenges that coastal areas face around the world, ultimately leading to more sustainable coastal environments.

Funding

No funding was received for this study

Conflicts of interest

The authors declare no conflicts of interest

Authors contribution statement

Ahmed S.A. Ibrahim: Data curation; Formal analysis; Investigation; Methodology; Software; Validation; Visualization; Roles/Writing – original draft

Anas M. El-Molla: Investigation; Methodology; Supervision; Validation; Visualization; Writing – review & editing.

Hany G.I. Ahmed: Investigation; Methodology; Supervision; Validation; Visualization; Writing – review & editing.

References

[1] Başaran B, Güner A, Anıl H. Effect of wave climate change on longshore sediment transport in Southwestern Black Sea. Estuar Coast Shelf Sci 2021;258. https://doi.org/10.1016/j.ecss.2021.107415.

[2] Arns A, Dangendorf S, Jensen J, Talke S, Bender J, Pattiaratchi C. Sea-level rise induced amplification of coastal protection design heights. Sci Rep 2017;7:1–9. https://doi.org/10.1038/srep40171.

[3] Grases A, Gracia V, García-León M, Lin-Ye J, Sierra JP. Coastal flooding and erosion under a changing climate: Implications at a low-lying coast (ebro delta). Water (Switzerland) 2020;12. https://doi.org/10.3390/w12020346.

[4] Knobler S, Liberzon D, Fedele F. Large waves and navigation hazards of the Eastern Mediterranean Sea. Sci Rep 2022;12:1–17.

https://doi.org/10.1038/s41598-022-20355-9.

[5] Satterthwaite D. The transition to a predominantly urban world and its underpinnings. Hum Settlements Discuss Pap Ser Urban Chang 2007:99p.

[6] Khalifa MA. Adoption of recent formulae for sediment transport calculations applied on the Egyptian Nile delta coastal area. J Coast Conserv 2011;16:37–49. https://doi.org/10.1007/s11852-011-0166-z.

[7] Nikmanesh MR, Talebbeydokhti N. Numerical simulation for predicting concentration profiles of cohesive sediments in surf zone. Sci Iran 2013;20:454–65. https://doi.org/10.1016/j.scient.2013.04.006.

[8] Remya PG, Kumar R, Basu S, Sarkar A. Wave hindcast experiments in the Indian Ocean using MIKE 21 SW model. J Earth Syst Sci 2012;121:385–92. https://doi.org/10.1007/s12040-012-0169-7.

[9] Moeini MH, Shahidi A. Application of two numerical models for wave hindcasting in Lake Erie. Appl Ocean Res 2007;29:137–45. https://doi.org/10.1016/j.apor.2007.10.001.

[10] Hadadpour S, Moshfeghi H, Jabbari E, Kamranzad B. Wave hindcasting in Anzali, Caspian Sea: a hybrid approach. J Coast Res 2013;65:237–42. https://doi.org/10.2112/si65-041.1.

[11] Keshtpoor M, Puleo JA, Shi F, DiCosmo NR. Numerical simulation of nearshore hydrodynamics and sediment transport downdrift of a tidal inlet. J Waterw Port, Coastal, Ocean Eng 2015;141. https://doi.org/10.1061/(ASCE)WW.1943-5460.0000273.

[12] SARAÇOĞLU K, ARI GÜNER H, ŞAHİN C, YÜKSEL Y, ÇEVİK E. Evaluation of the wave climate over the black sea: field observations and modeling. Coast Eng 2016:2013–5. https://doi.org/10.9753/icce.v35.waves.20.

[13] Barbariol F, Davison S, Falcieri FM, Ferretti R, Ricchi A, Sclavo M, et al. Wind Waves in the Mediterranean Sea: An ERA5 Reanalysis Wind-Based Climatology. Front Mar Sci 2021;8:1–23. https://doi.org/10.3389/fmars.2021.760614.

[14] IPCC. Climate Change 2022: Impacts, Adaptation and Vulnerability. Contribution of Working Group II to the Sixth Assessment Report of the Intergovernmental Panel on Climate Change [H.-O. Pörtner, D.C. Roberts, M. Tignor, E.S. Poloczanska, K. Mintenbeck, A. Alegr. Cambridge Univ Press Cambridge Univ Press Cambridge, UK New York, NY, USA 2022;3056 pp. https://doi.org/10.1017/9781009325844.

[15] Amarouche K, Akpınar A, Bachari NEI, Çakmak RE, Houma F. Evaluation of a high-resolution wave hindcast model SWAN for the West Mediterranean basin. Appl Ocean Res 2019;84:225–41. https://doi.org/10.1016/j.apor.2019.01.014.

[16] Simav Ö, Şeker DZ, Gazioğlu C. Coastal inundation due to sea level rise and extreme sea state and its potential impacts: Çukurova Delta case. Turkish J Earth Sci 2013;22:671–80. https://doi.org/10.3906/yer-1205-3.

[17] Sharaan M, Ibrahim MG, Moubarak H, Elkut AE, Romya AA, Hamouda M, et al. A Qualitative Analysis of Climate Impacts on Egyptian Ports. Sustainability 2024;16:1015. https://doi.org/doi.org/10.3390/su16031015.

[18] Van Rijn LC, Professor JSRA, Engineer JVDW, J.R. D. Coastal sediment dynamics: recent advances and future research needs. J Hydraul Res 2013;51:475–93. https://doi.org/10.1080/00221686.2013.849297.

[19] Chen, J.-L., Hsu, T.-J., Shi F, Raubenheimer, et al. Hydrodynamic and sediment transport modeling of New River Inlet (NC) under the interaction of tides and waves. J Geophys Res Ocean 2015;120:4028–4047. https://doi.org/10.1002/2014JC010425.

[20] ASRT. Sedimentation in Damietta Harbor; Academy of Scientific Research and Technology Final Report; ASRT: Cairo, Egypt. 1988.

[21] El Asmar HM, White K. Changes in coastal sediment transport processes due to construction of New Damietta Harbour, Nile Delta, Egypt. Coast Eng 2002;46:127–38. https://doi.org/10.1016/S0378-3839(02)00068-6.

[22] Sogreah M. Effects on the construction of the Port of Damietta on the evolution of the littoral drift. Consult Report, Number 35/1202/R9 1982:35.

[23] Khalifa AM, Soliman MR, Yassin AA. Assessment of a combination between hard structures and sand nourishment eastern of

Damietta harbor using numerical modeling. Alexandria Eng J 2017;56:545–55. https://doi.org/10.1016/j.aej.2017.04.009.

[24] Hesham M. El-Asmar, Maysa M.N. Taha ASE-S. Morphodynamic changes as an impact of human intervention at the Ras El-Bar-Damietta Harbor coast, NW Damietta Promontory, Nile Delta, Egypt. J African Earth Sci 2016;124:323–39. https://doi.org/10.1016/j.jafrearsci.2016.09.035.

[25] El-Fishawi N. Relative changes in sea level from tide gauge records at Burrulus, central part of the Nile Delta coast. INQUA MBSS Newsl 1994;16:53 – 61.

[26] Eid FM, El-Din SHS, El-Din KAA. Sea level variation along the Suez Canal. Estuar Coast Shelf Sci 1997;44:613–9. https://doi.org/10.1006/ecss.1996.0160.

[27] DHI. Introducting the MIKE 21 Shoreline Morphology Module, Denmark, DHI Headquarters 2017.

[28] DHI. MIKE 21 & MIKE 3 Flow Model FM - Hydrodynamic Module, Denmark, DHI Headquarters 2017.

[29] DHI. MIKE 21 Wave Modelling - MIKE 21 Spectral Waves FM, Denmark, DHI Headquarters 2017.

[30] Komen GJL, Cavaleri M, Donelan K, Hasselmann S, PAEM J. Dynamics and Modelling of Ocean Waves. Cambridge Univ Press 1994;UK:560.

[31] Young IR. Wind generated ocean waves. Elsevier 1999;2.

[32] DHI. MIKE 21 & MIKE 3 Flow Model FM - Sand Transport Module, Denmark, DHI Headquarters 2017.

[33] Sen PK. Estimates of the Regression Coefficient Based on Kendall's Tau. J Am Stat Assoc 1968;63:1379–89. https://doi.org/10.1080/01621459.1968.10480934.

[34] Yue S, Pilon PJ, Cavadias G. Power of the Mann–Kendall and Spearman's rho tests for detecting monotonic trends in hydrological series. J Hydrol 2002;259:254–71. https://doi.org/10.1016/S0022-1694(01)00594-7.

[35] Aarnes OJ, Abdalla S, Bidlot JR, Breivik Ø. Marine wind and wave height trends at different ERA-interim forecast ranges. J Clim 2015;28:819–37. https://doi.org/10.1175/JCLI-D-14-00470.1.

[36] Abo Zed A. Effects of waves and currents on the siltation problem of Damietta harbour, Nile Delta coast, Egypt. Mediterr Mar Sci 2007;8:33–48. https://doi.org/10.12681/mms.152.

[37] Frihy OE, Abd El Moniem AB, Hassan MS. Sedimentation processes at the navigation channel of the Damietta Harbour on the Northeastern Nile Delta coast of Egypt. J Coast Res 2002;18:459–69.

[38] Tech. T. Shoreline master plan for the Nile Delta coast. Prog Rep Number 1 1984:143.

[39] El-Asmar HM, White K. Rapid updating of maps of dynamic coastal landforms by segmentation of Thematic Mapper imagery, example from the Nile Delta, Egypt. Proc 23rd Annu Conf Remote Sens Soc 1997:515 – 520.